Journal of ELECTRONIC MATERIALS, Vol. 47, No. 6, 2018
https://doi.org/10.1007/s11664-017-5959-x

TOPICAL COLLECTION: INTERNATIONAL CONFERENCE ON THERMOELECTRICS 2017

The Influence of the Inner Topology of Cooling Units on the Performance of Automotive Exhaust-Based Thermoelectric Generators

D.C. ZHU,[1] C.Q. SU,[1] Y.D. DENG,[1] Y.P. WANG,[1,2,3] and X. LIU[1]

1.—Hubei Key Laboratory of Advanced Technology for Automotive Components, Automobile Engineering Institute, Wuhan University of Technology, 205 Luoshi Road, Hongshan District, Wuhan 430070, China. 2.—e-mail: wangyiping@whut.edu.cn. 3.—e-mail: 309166259@qq.com

Automotive exhaust-based thermoelectric generators are currently a hot topic in energy recovery. The waste heat of automotive exhaust gas can be converted into electricity by means of thermoelectric modules. Generally, inserting fins into the cooling unit contributes to enhancing the heat transfer for a higher power output. However, the introduction of fins will result in a pressure drop in the cooling system. In current research, in order to enhance the heat transfer and avoid a large pressure drop, a cooling unit with cylindrical grooves on the interior surface was proposed. To evaluate the performance of the cylindrical grooves, different inner topologies, including a smooth interior surface,a smooth interior surface with inserted fins and an interior surface with cylindrical grooves, were compared. The results revealed that compared with the smooth interior surface, the smooth interior surface with inserted fins and the interior surface with cylindrical grooves both enhanced the heat transfer, but the interior surface with cylindrical grooves obtained a lower pressure drop. To improve the performance of the cylindrical grooves, different groove-depth ratios were tried, and the results showed that a groove-depth ratio of 0.081 could provide the best overall performance.

Key words: TEG, cooling unit, numerical simulation, cylindrical grooves

INTRODUCTION

Thermoelectric energy conversion is a reliable and environmentally friendly technology, which has been used in military and deep space exploration for many years. With the rapid development of semiconductor materials, this technology has begun to be applied in other engineering domains, such as in the auto industry. Generally, about 40% of fuel energy is discharged in the form of waste heat in the exhaust gas. Thermoelectric generators can be used in automobiles to recover this huge waste heat energy with advantages of zero emission, no noise, and no mechanical vibration. because of these merits, TEG has received increasing attention in the recovery of engine waste heat.[1,2]

Thacher et al.[3] installed a 16-module TEG in a pick-up truck with a 5.3L V-8 gasoline engine and obtained 255 W power output. Crane et al.[4] built and tested a 125 W high-temperature segmented-element TEG. Liu et al.[5] designed a "four-TEG" system and assembled it into a medium off-road vehicle. A maximum power of 944 W was obtained. Yang[6] reported the possibility of generating an average of 350 W during Federal Test Procedure (FTP) cycles with a TEG installed in a conventional full-size truck. To improve the performance of the TEG, increasing attention is paid to improve the performance of the hot-side, that is, the heat exchanger. For instance, Deng[7,8] constructed different heat exchangers, including maze-shaped, fish-bone-shaped and chaos-shaped heat exchangers, to analyze their thermal performance in TEGs. Wang

(Received July 28, 2017; accepted November 14, 2017; published online November 20, 2017)

et al.[9,10] optimized the fin distribution and discussed different inner topologies in heat exchangers to improve the temperature uniformity of a heat exchanger in a TEG. To enhance the heat transfer with lower pressure loss in the heat exchanger, a dimpled non-smooth surface was also introduced in the heat exchanger.[11,12] Kumar[13] analyzed the influence of heat exchanger, geometry, and thermoelectric module configurations on the performance of TEG.

Obviously, the research related to the hot-side of TEG has made great progress and truly improved the overall performance. However, for TEG, the heat transfer on the cold-side is equally important. For instance, Thacher et al.[3] concluded that the thermoelectric efficiency could be improved by decreasing the temperature of the cold-side. Rezania[14] found that there was a unique flow rate that gave maximum net output power in the TEG at each temperature difference. Su et al.[15] analyzed the influence of three different cooling unit configurations called plate-shape, stripe shape, and diamond-shape on the performance of the TEG, and found that the diamond-shaped achieved a better performance. Su et al.[16] also found that the parallel connection of cooling units was more appropriate than series connection. Qiang et al.[17] revealed that the cooling efficiency could be improved by changing the layout of fins in the cavity. For heat transfer enhancement, Eiamas-ard et al.[18] found that the heat transfer can be enhanced by rib-groove arrangements. Bi et al.[19] revealed that cylindrical grooves had a good performance in heat transfer enhancement. In the present study, in order to obtain more power generation and avoid high pressure drop, a cooling unit with cylindrical grooves on the interior surface was proposed. The performance of the TEGs with different cooling units, such as cooling units with flat interior surfaces, cooling units with inserted fins and cooling units with cylindrical grooves, were discussed. Furthermore, the effect of the different groove-depth ratios (the channel hydraulic diameter divided by the groove depth) on the heat transfer performance of the cooling units were also studied. Finally, a cooling unit that could improve the output power of TEG but had a low pressure drop was obtained.

NUMERAL SIMULATION

Geometry

The layout of the automotive exhaust-based TEG was plotted in Fig. 1. The whole structure of the TEG was an octadecagon. Three hundreds and six TEMs were mounted on the outer surface of the heat exchanger with 17 modules on each side. In addition, the cold sides of TEMs were in close contact with the external flat plane of the cooling unit. Furthermore, the heat exchanger, TEMs and cooling units were bound by clamping rings, which

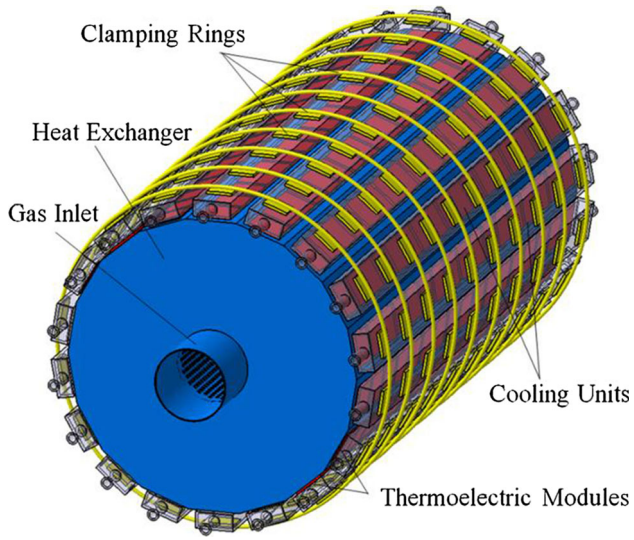

Fig. 1. The geometry of the cylindrical TEG.

were made from spring steel. Compared with the conventional flat-form TEG, cylindrical TEG was better to distribute and manage the thermal expansion forces,[4] and more likely to integrate with the muffler, three-way catalytic converter or selective catalytic reduction (SCR).[20]

Because of the axial symmetry of the whole structure, one ninth of the TEG was taken as the research object. To investigate the influence of inner topology of cooling units on the TEG performance, three different cooling units with different inner topologies were proposed (see Fig. 2). The inner topologies included a flat interior surface (A0), an interior surface with fins arranged transversely (A1) and interior surfaces with cylindrical grooves (A2). For A1, transversely arranged fins have been proved to be effective in heat transfer enhancement. For A2, the streamwise span of grooves was 8 mm and the groove-depth ratio was 0.069. Related research revealed that the groove-depth had a great influence on the heat transfer.[21] Therefore, to investigate the influence of groove-depth ratio on the heat transfer, another two cooling units with groove-depth ratios of 0.081 (B0) and 0.102 (B1) were proposed.

In general, there are four forms of heat transfer, including heat conduction, forced heat convection, natural heat convection and heat radiation. Because heat radiation was relatively too low in this study, it was omitted. As shown in Fig. 3, firstly, the heat transfer between exhaust gas and inner surfaces of the heat exchanger was forced heat convection. Then, the heat transfer from the hot sides to cold sides of modules was heat conduction. Subsequently, the heat was transferred between cooling water and inner surfaces of cooling unit by forced heat convection. Meanwhile, the heat transfer between the external surface of TEG and ambient air was natural heat convection.

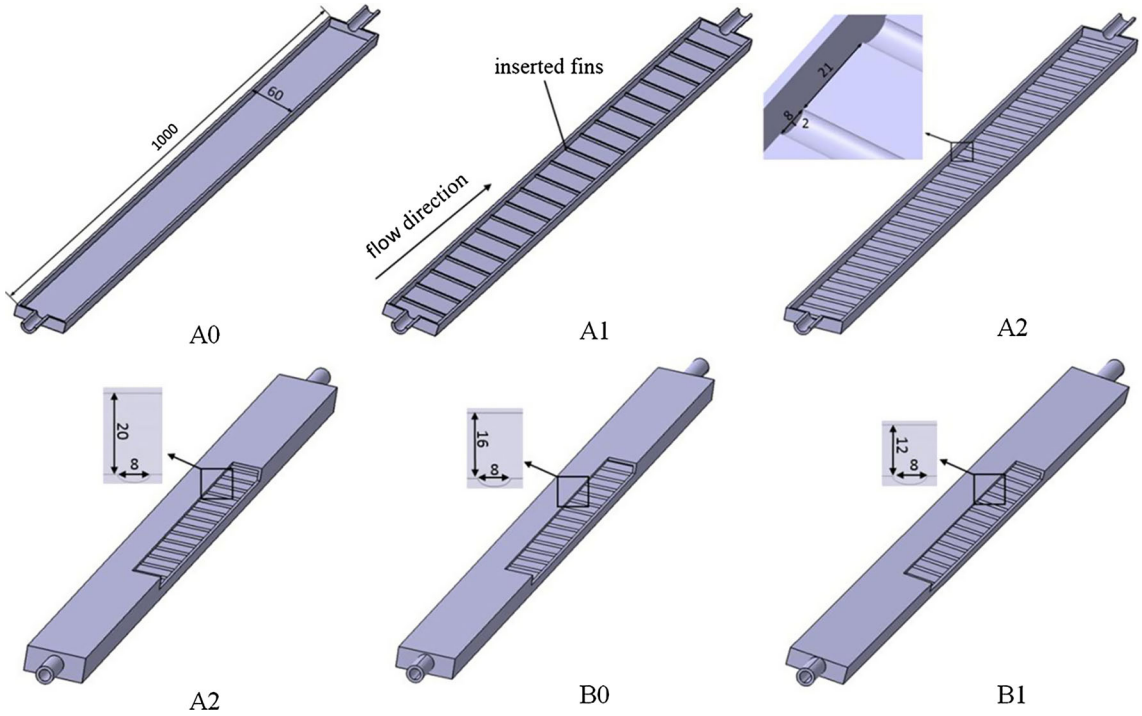

Fig. 2. The cooling units with different inner topologies (units: mm).

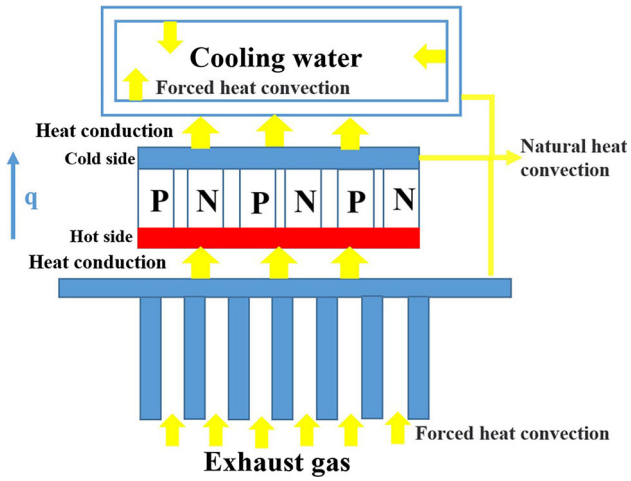

Fig. 3. Schematic of TEG model.

Turbulence Model and Boundary Conditions

The k–ε turbulence model has become the most widely used industrial model because of its low computational resource demand, fast numerical convergence, data stability and high accuracy. Compared to other k–ε turbulence models, the realizable k-ε turbulence model can keep the simulation results highly consistent with the Reynolds stress in real turbulence and shows greater capacity in the computation of secondary flow or flow separation. Considering the secondary flow in this study, the realizable k-ε turbulence model was selected to predict the flow and temperature field inside the TEG in the current research. To simplify the simulation, the fluid was considered as incompressible, the flow was steady and no phase transition occur in the TEG. In addition, the molecular viscosity can be neglected in the fully turbulent fluid, and the thermal contact resistance can be ignored since the contact between different parts of the TEG was reliable. Therefore, the transport equations for turbulence kinetic energy k and dissipation rate of turbulence energy ε could be written as:

$$\frac{\partial(ku_j)}{\partial x_j} = \frac{1}{\rho}\frac{\partial}{\partial x_j}\left[\left(\mu + \frac{\mu_t}{\sigma_k}\right)\frac{\partial k}{\partial x_j}\right] + \frac{1}{\rho}G_k - \varepsilon \quad (1)$$

$$\frac{\partial(\varepsilon u_j)}{\partial x_j} = \frac{1}{\rho}\frac{\partial}{\partial x_j}\left[\left(\mu + \frac{\mu_t}{\sigma_\varepsilon}\right)\frac{\partial \varepsilon}{\partial x_j}\right] + C_1 S\varepsilon - C_2\frac{\varepsilon^2}{k + \sqrt{v\varepsilon}} \quad (2)$$

where x_j is the position vector and ρ is referred to the fluid density. μ_t is the turbulent eddy viscosity, μ is the kinetic viscosity, u_j is the velocity vector, k is the turbulent kinetic energy, G_k is the turbulence kinetic energy created by laminar velocity gradient, S is the modulus of the mean rate-of-strain tensor, v is kinetic viscosity, C_1, C_2, σ_k and σ_ε are constants.

The energy equation in turbulent heat transfer is given by:

$$\frac{\partial}{\partial x_i}[u_i(\rho E + p)] = \frac{\partial}{\partial x_j}\left[k_{\text{eff}}\frac{\partial T}{\partial x_j} + u_i(\tau_{ij})_{\text{eff}}\right] + S_h \quad (3)$$

$$k_{\text{eff}} = k_1 + k_t \tag{4}$$

$$E = h - \frac{p}{\rho} + \frac{v_1^2}{2} \tag{5}$$

where E is the total energy, p is the pressure, k_{eff} is the effective thermal conductivity, k_1 is the thermal conductivity, k_t is the turbulent thermal conductivity, T is temperature, $(\tau_{ij})_{\text{eff}}$ is the deviatoric stress tensor, S_h is volumetric heat source, h is enthalpy, and v_1 is velocity. Moreover, all simulations were carried out using the commercial software ANSYS FLUENT.

Based on the bench test experiment, the temperature of the inlet flow was set to 773 K at a mass flow of 0.0037 kg/s. As the muffler had been integrated into the heat exchanger, and the exit of the exchanger was connected to the atmosphere directly, the pressure at the outlet was 0 Pa. In addition, the coefficient of convective heat transfer between the external surface of the heat exchanger and the ambient air was set to 10 W/(m^2 K) with the environmental temperature being set to 300 K.[22] Considering the temperature of the circulation coolant in the engine cooling system ranged from 330 K to 360 K at the outlet of the radiator, the inlet temperature of the cooling unit was set to 333 K. According to the capacity of the pump in the test bench, the average velocity at the inlet of the single cooling unit was set to 1 m/s and the pressure was set to zero at the outlet as well. As the counter flow arrangement could obtain a higher output power of the TEG than the co-flow arrangement, the counter flow arrangement was adopted in current research.[23]

Computation Validation

To check the mesh independence, three different grid numbers were employed, namely 4.2 million, 6.9 million, and 8.3 million. The mean streamwise temperature variations at the hot sides of the TEMs revealed that the results obtained by the 8.3 million grid had a good agreement with the 6.9 million grid (See Fig. 4). By considering the computational cost and efficiency, the computational model with a grid number of 6.9 million was used.

To validate further the computational results, a test bench was constructed to measure the temperature distribution on the surface of the heat exchanger. As shown in Fig. 5, the test bench consisted of a TEG, a catalytic converter and a 2.0 L gasoline engine whose parameters are listed in Table I. During measurements, the engine speed was maintained at 4000 rpm and the output power was about 40 kW. In order to measure the temperature distribution, several K-type thermocouples were installed on the surface of the heat exchanger, and the temperatures at 17 points along one side of the cylindrical TEG were measured.

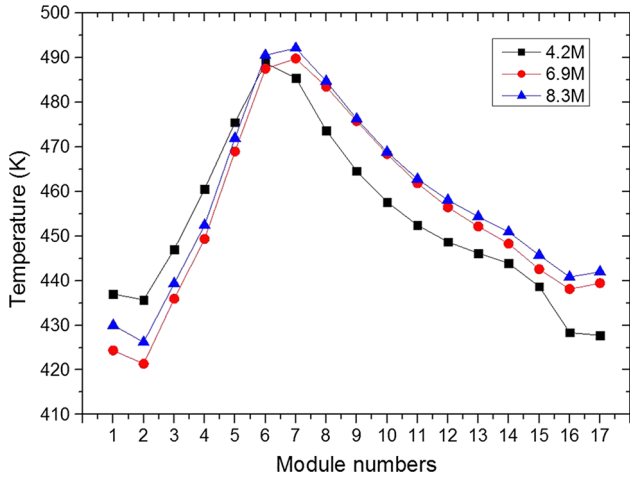

Fig. 4. The mean streamwise temperature of the hot sides of the TEMs .

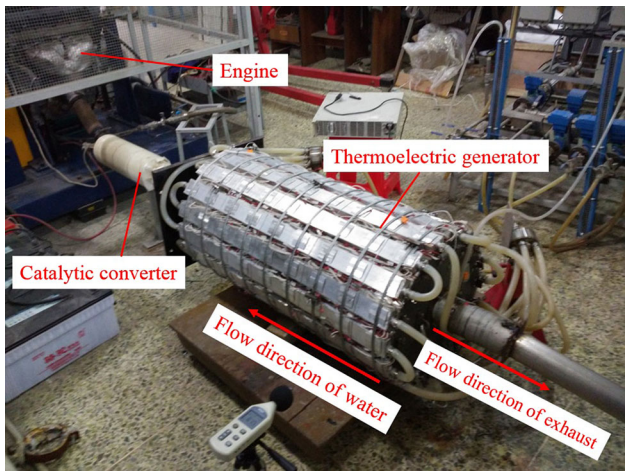

Fig. 5. Cylindrical thermoelectric generator test bench.

The temperature comparison between the measurements and computation plotted in Fig. 6 revealed that the computational results had a good agreement with the experimental data, and the possible error sources were: (1) the inlet temperatures and mass flow rate of coolant and exhaust gas were difficult to keep unchanged in experiment, while these parameters were considered to be unchanged in the computation; (2) the ambient temperature in the experiment was fluctuated but constant in the computation; (3) measurement errors such as instrument errors and reading errors.

Results and Discussion

The flow structure and turbulent kinetic energy (TKE) on the spanwise plane ($x = -0.05$) for A2 (see Fig. 7) showed that a large transverse vortex, which strengthened the turbulent mixing could be found in the spanwise section. As shown in the TKE

Table I. The engine performance parameters

Parameter	Value	Parameter	Value
Cylinder number	4	Maximum power/speed	108 kW/6000 rpm
Valves per cylinder	4	Peak torque/speed	200 N m/4000 rpm
Displacement	1997 mL	Power of pump	0.18 kW
Bore/stroke	85/88 mm	Cooling mode	Water cooling
Radiator size	547 × 415 × 50 mm	Number of fan shift	1

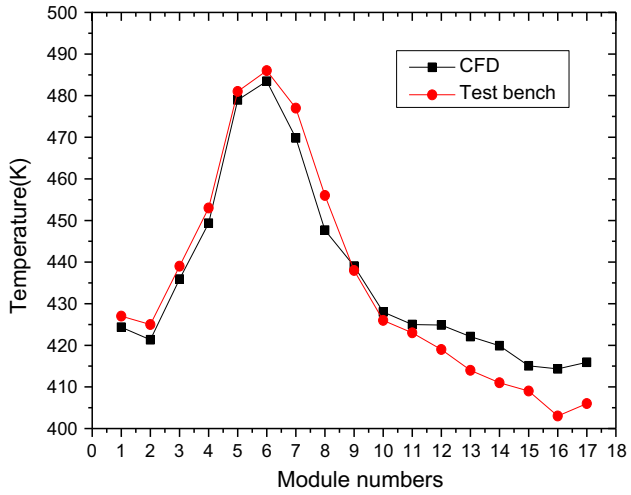

Fig. 6. Temperature at the measurement points obtained by CFD and experiment.

distribution, the turbulent mixing was stronger in A2, and the cylindrical grooves could make the boundary layer around the edges thinner and enhance the amount of turbulent flow in the fluid. For A1, the flow on the spanwise plane was almost upward and downward flows, and the transverse flow mixing nearly disappeared. However, structures such as fins can induce strong flow impingement and the large scale recirculation flow behind the structures, leading to high TKE in A1. The TKE distribution showed that the turbulent kinetic values in A1 were the largest, which induces the largest pressure loss penalty. The results proved that the cylindrical grooves and the fins can both increase the turbulent kinetic energy and increase the heat transfer area, which is favorable to the heat transfer enhancement.

The Nusselt number and friction coefficient at the bottom coupling surfaces plotted in Fig. 8 showed that the Nusselt number increased with the friction coefficient accordingly, and the distribution of the Nusselt number was more uniform than the distribution of the friction coefficient, especially in the high-velocity area. In addition, the higher friction coefficient zone was mainly concentrated at the inlet and outlet of the cooling unit, where the flow velocity was also higher. As a result, the friction coefficient was more sensitive to the change of fluid velocity. As shown in Fig. 8a, heat transfer enhancement by fins (A1) was similar to that of cylindrical grooves (A2). However, for the geometries such as fins (A1), the pressure drop was larger and flow impingement and recirculation which would induce fiction coefficient were stronger.

To further compare the performance of cooling unit with different inner topologies, the area-averaged Nusselt number and friction coefficient at the coupling surface were extracted (see Fig. 9). Compared with A0, the Nusselt number of A1, A2, B0 and B1 increased by 51.7%, 41.7%, 71.9%, and 85.8%, respectively. However, compared with A0,the averaged friction coefficient of A1, A2, B0 and B1 increased by 15.0%, 6.8%, 62.6%, and 158.3%, respectively.

In order to evaluate the efficiency of heat transfer, a comprehensive efficiency factor η was used as

$$\eta = \left(\frac{Nu}{Nu_0}\right) \Big/ \left(\frac{f}{f_0}\right) \tag{6}$$

where Nu_0 and f_0 are the coupling surface averaged Nusselt number and friction coefficient in the flat channel (A0), respectively.

As shown in Fig. 9, the cylindrical grooves (A2) had similar heat transfer enhancement performance as the inserted fins (A1) while the friction coefficient in A2 decreased. Although the coupling surface averaged Nusselt number of cylindrical grooves (A2) was slightly smaller than that of inserted fins (A1), the comprehensive efficiency factor of the cylindrical grooves was higher (see Fig. 10). Therefore, the overall thermal performance of the cylindrical grooves was better. As for the groove-depth ratio, a higher ratio led to higher surface Nusselt numbers and higher surface friction coefficient, and a groove-depth ratio of 0.081 (B0) provided the best overall performance.

Figure 11 showed the mean temperatures of two sides of TEMs and the mean temperature difference between the hot side and cold side of each module on one side of the TEG. We noticed that the impact of the inner topology of the cooling unit on the temperature of cold sides of the TEMs was much greater than that on the hot side. Therefore, we concluded that the increase of the temperature difference between the hot side and cold side of each

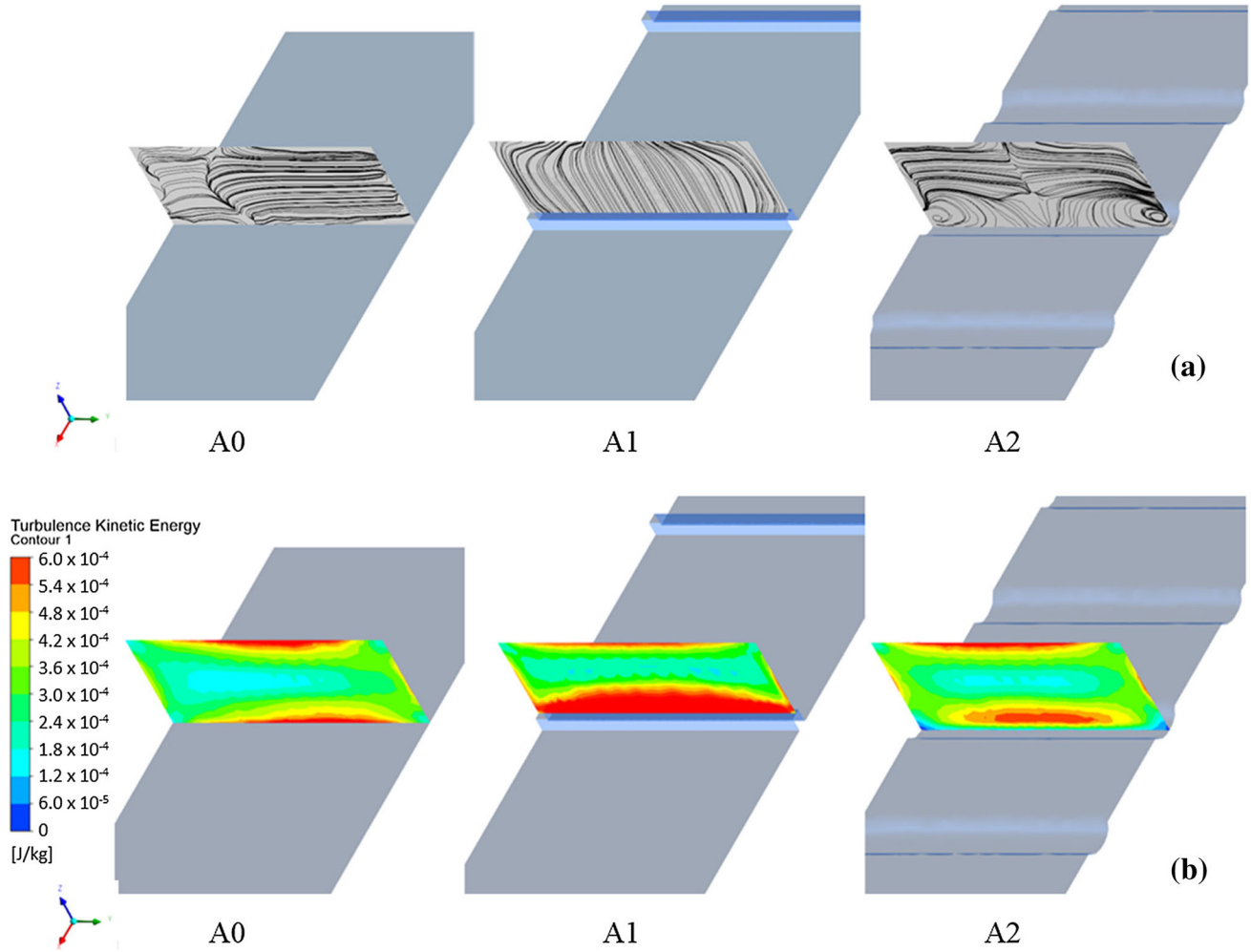

Fig. 7. (a) Streamline contours on the spanwise plane ($x = -0.05$) and (b) turbulent kinetic energy (TKE) for A0, A1 and A2.

module is mainly attributed to the temperature decrease on the cold side.

OUTPUT PERFORMANCE OF THE TEG

Performance Parameters of the TEM and the TEG

According to the fundamental formula of the Seebeck effect

$$U_o = N \cdot \alpha_{PN} \cdot (T_h - T_c) = N \cdot (\alpha_P - \alpha_N) \cdot (T_h - T_c) \tag{7}$$

where U_o is the module open-circuit voltage, N is the number of thermocouples, α_{PN} is the relative Seebeck coefficient, i.e. the difference between α_P and α_N, which depends on the characteristics of the thermoelectric materials, and T_h and T_c are the temperatures of the hot and cold sides of the TEMs.

The internal resistance of the modules R_{in} is given as follow:

$$R_{in} = Nr_o = N\left(\frac{\rho_N l_N}{A_N} + \frac{\rho_P l_P}{A_P}\right) \tag{8}$$

where l_N and l_P are the thermoelectrical length of the n-type and p-type materials, respectively, ρ_N and ρ_P are the electrical resistivities of the n-type and p-type materials, respectively, and A_N and A_P are the cross-sectional area of the n-type and p-type thermocouple, respectively.

According to the previous study,[15] the output power will reach the maximum when the electronic load resistance was equal to the internal resistance of the modules. The output power could be described as:

$$P_{\text{teg}} = U_o^2 / \frac{(R_L + R_{in})^2}{R_L} \tag{9}$$

and the maximum output power could be obtained as:

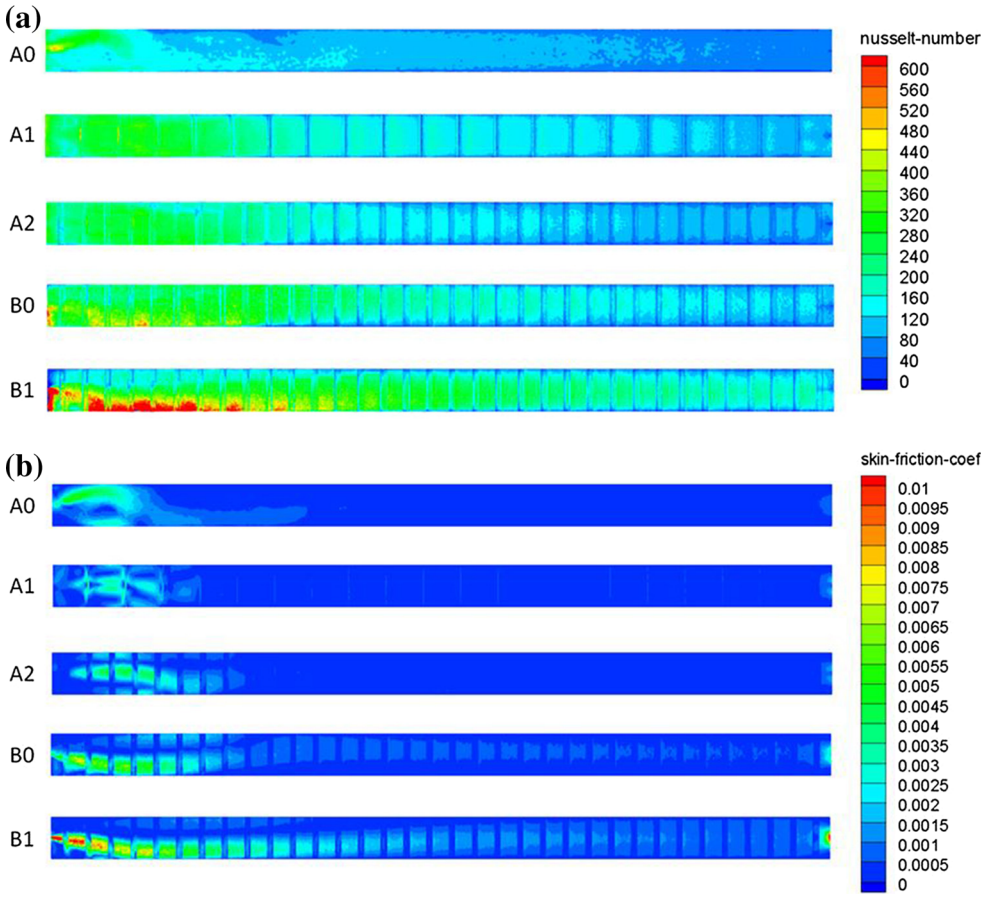

Fig. 8. Nusselt number contours (a) and skin friction coefficient contours (b) on the bottom coupling wall of the cooling units.

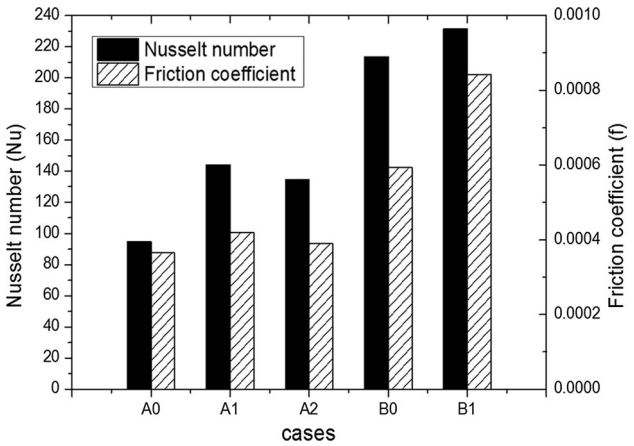

Fig. 9. Averaged Nusselt numbers and averaged friction coefficients on the coupling walls of the cooling units.

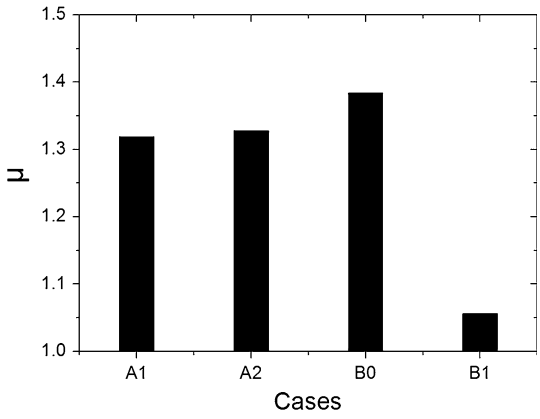

Fig. 10. The comprehensive efficiency factor of η in different cases.

$$P_m = \frac{U_o^2}{4R_{in}} \tag{10}$$

where R_L is the electrical load resistance and P_m is the maximum output power.

In this study, seventeen TEMs were connected in series. For TEMs connected in series, the open circuit voltage, internal resistance and maximum output power of the TEG were as follows:

$$U_o = \sum_{i=1}^{17} U_i \tag{11}$$

$$R_{in} = \sum_{i=1}^{17} R_i \tag{12}$$

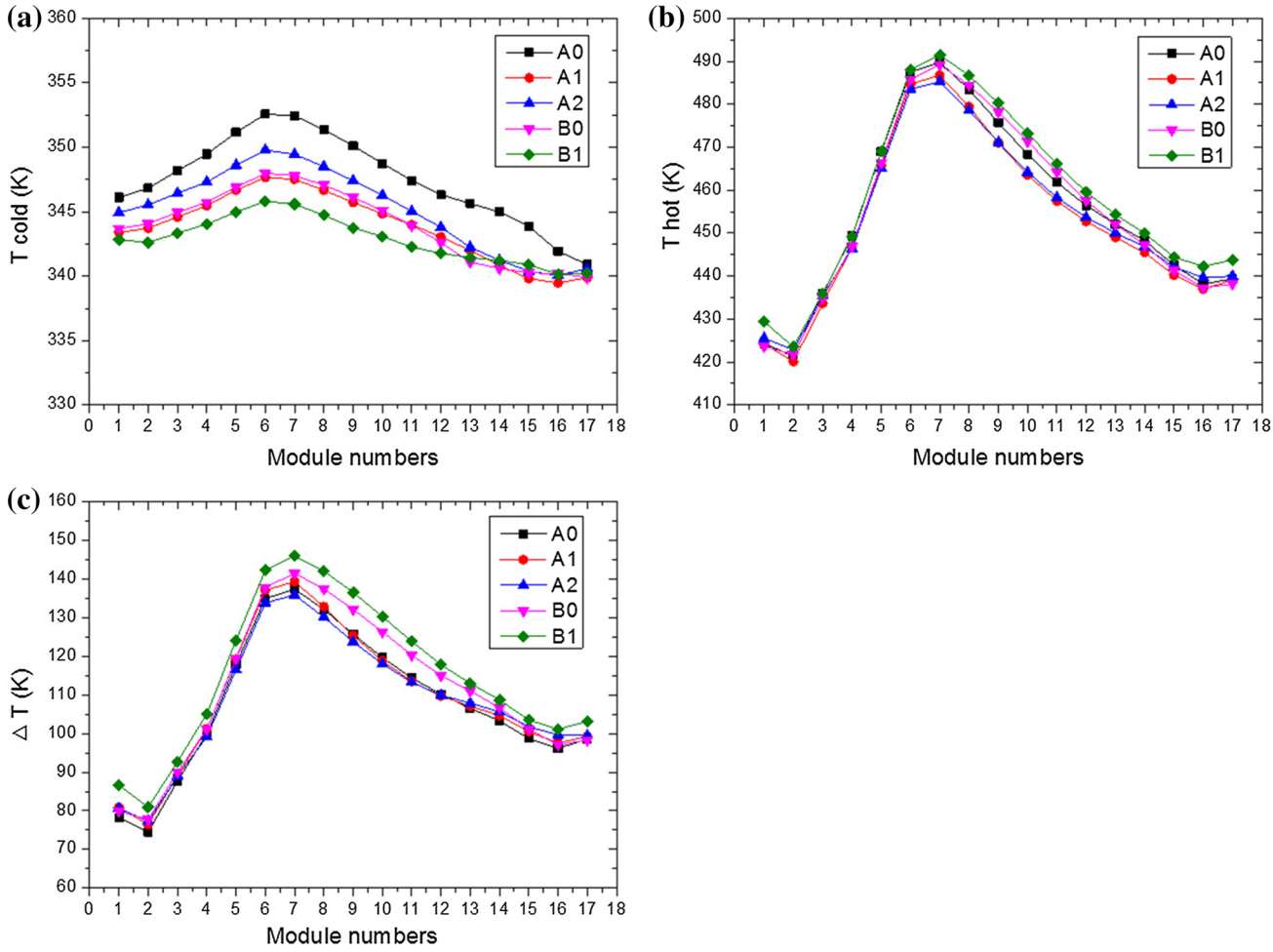

Fig. 11. (a) Mean temperature distribution of the cold side of TEM; (b) mean temperature distribution of the hot side of TEM; (c) mean temperature difference distribution of TEM.

Table II. Parameters of *p-n* materials

Parameter	*p*-type	*n*-type
Seebeck coefficient, S^j (μV/K)	215	− 215
Electrical resistivity, q^j (Ω m)	1.04×10^{-5}	1.04×10^{-5}
Thermal conductivity, k^j [W/((mK)]	1.5	2.5
Z (K^{-1})	0.2×10^{-3}	2.85×10^{-3}
Height, H (m)	0.005	0.005

$$P_{\mathrm{TEGm}} = \frac{\left(\sum_{i=1}^{17} U_i\right)^2}{4\sum_{i=1}^{17} R_i} \tag{13}$$

Modeling and Results

According to the parameters of TEM (see Table II) and Eq. 12, a mathematical model for the output power of the TEG based on MATLAB/SIMULINK was established, as shown in Fig. 12. Based on the temperature difference obtained by CFD, the output power was obtained. The final output power (Fig. 13) revealed that, compared with A0, the total power generation of B0 (about 656 W) increased by 5.6% while the pressure loss only increased by 3.3%. B0 provided a great overall performance, which agreed well with the conclusion in "Results and Discussion". The output power of the TEG in case B1 was the highest while its pressure drop increased by 12% than that in A0. With the increase

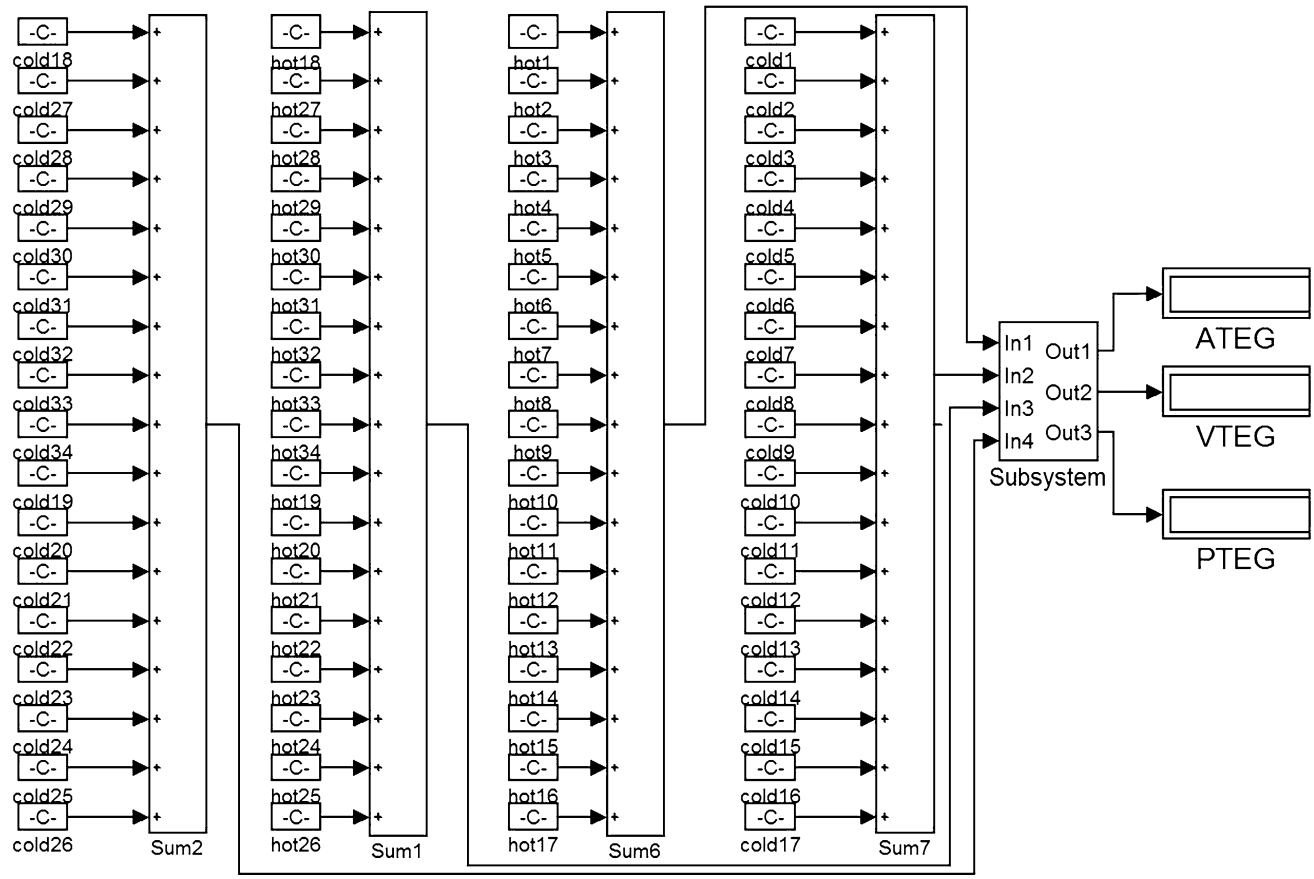

Fig. 12. Simulink mathematical model for output power of the TEG.

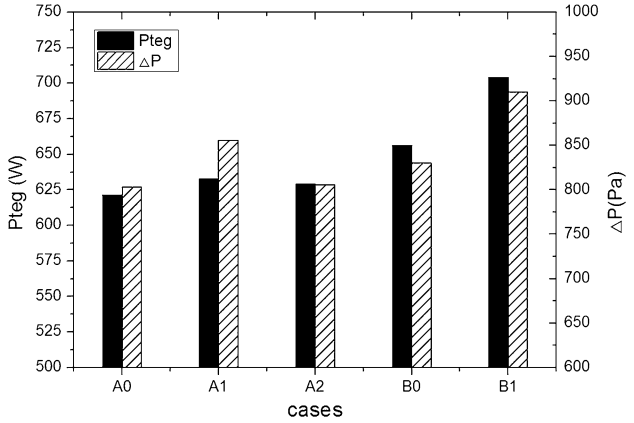

Fig. 13. Power generation and pressure drop in different cases.

of the groove-depth ratio, the output power increases, but the pressure loss also increases quickly.

CONCLUSIONS

The influence of different inner topologies of the cooling units on the performance of the TEG has been studied by numerical simulation. Three different inner configurations, namely flat interior surface (A0), interior surface with fins arranged transversely (A1) and cylindrical grooves (A2), were compared. Furthermore, the influence of groove-depth ratios on the performance of the TEG was also investigated. To validate the computation method, a test-bench was constructed to measure the temperature distribution on the surface of the cylindrical heat exchanger.

Simulation results showed that the inner configuration and the groove-depth ratio has an impact on the performance of the TEG. Compared to the flat interior surface, interior surface with fins or cylindrical grooves could both enhance the heat transfer and power generation but increase the pressure drop, while the pressure drop increment of the interior surface with cylindrical grooves was relatively low. An evaluation parameter was used to express the overall performance of the cooling unit. Finally, a cooling unit with cylindrical grooves and the groove-depth ratio of 0.081 (B0) provides the best overall performance. Furthermore, based on the mathematical model for the output power, 656.3 W could be obtained by the cylindrical TEG in case B0.

ACKNOWLEDGEMENTS

This work was supported by the Excellent Dissertation Cultivation Funds of Wuhan University of Technology (Grant No. 2016-YS-054), the Fundamental Research Funds for the Central Universities (WUT: 2017II18XZ) and the National Natural Science Foundation of China (Grant No. 51775395).

REFERENCES

1. R. Saidur, N.A. Rahim, H.W. Ping, M.I. Jahirul, S. Mekhilef, and H.H. Masjuki, *Energy Policy* 37, 3650 (2009).
2. Y. Wang, C. Dai, and S. Wang, *Appl. Energy* 112, 1171 (2013).
3. E.F. Thacher, B.T. Helenbrook, M.A. Karri, and C.J. Richter, *Proc. Inst. Mech. Eng.* 221, 95 (2007).
4. D.T. Crane and J.W. Lagrandeur, *J. Electron. Mater.* 39, 2142 (2010).
5. X. Liu, Y.D. Deng, Z. Li, and C.Q. Su, *Energy Convers. Manag.* 90, 121 (2015).
6. J. Yang, *Proceedings of 24th International Conference on Thermoelectrics* (2005), pp. 170–174.
7. Y.D. Deng, X. Liu, S. Chen, and N.Q. Tong, *J. Electron. Mater.* 42, 1634 (2012).
8. X. Liu, C.G. Yu, S. Chen, Y.P. Wang, and C.Q. Su, *J. Electron. Mater.* 43, 2218 (2014).
9. Y.P. Wang, C. Wu, Z.B. Tang, X. Yang, Y.D. Deng, and C.Q. Su, *J. Electron. Mater.* 44, 1724 (2015).
10. Y.P. Wang, S. Li, X. Yang, Y.D. Deng, and C.Q. Su, *Energy. Convers. Manag.* 126, 266 (2016).
11. S. Li, Y.P. Wang, T. Wang, X. Yang, Y.D. Deng, and C.Q. Su, *J. Electron. Mater.* 46, 3062 (2017).
12. Y.P. Wang, S. Li, Y.D. Deng, and C.Q. Su, *J. Electron. Mater.* 45, 1792 (2016).
13. S. Kumar, S.D. Heister, X. Xu, J.R. Salvador, and G.P. Meisner, *J. Electron. Mater.* 42, 944 (2013).
14. A. Rezania, L.A. Rosendahl, and S.J. Andreasen, *Int. Commun. Heat Mass* 39, 1054 (2012).
15. C.Q. Su, M. Xu, W.S. Wang, Y.D. Deng, X. Wang, and Z.B. Tang, *J. Electron. Mater.* 44, 1 (2015).
16. C.Q. Su, D.C. Zhu, Y.D. Deng, Y.P. Wang, and X. Liu, *J. Electron. Mater.* 46, 2822 (2017).
17. J.W. Qiang, C.G. Yu, Y.D. Deng, C.Q. Su, Y.P. Wang, and X.H. Yuan, *J. Electron. Mater.* 45, 1679 (2016).
18. S. Eiamsa-ard and P. Promvonge, *Int. Commun. Heat Mass Transfer* 35, 844 (2008).
19. C. Bi, G.H. Tang, and W.Q. Tao, *Appl. Therm. Eng.* 55, 121 (2013).
20. Y.D. Deng, Y.L. Chen, S. Chen, W.D. Xianyu, and C.Q. Su, *J. Electron. Mater.* 44, 1524 (2015).
21. A.A. Ramadhan, Y.T.A. Anii, and A.J. Shareef, *Heat Mass Transf.* 49, 185 (2013).
22. J.P. Holman, *Heat Transfer*, 9th ed. (New York: McGraw-Hill, 2002), p. 11.
23. Q. Du, H. Diao, Z. Niu, G. Zhang, G. Shu, and K. Jiao, *Energy Convers. Manag.* 101, 9 (2015).